Symmetrical Stabilization of Bound Ca^{2+} Ions in a Cooperative Pair of EF-Hands through Hydrogen Bonding of Coordinating Water Molecules in Calbindin D_{9k}†

Jonas Fast,*,‡ Maria Håkansson,§ Andreas Muranyi,‡,|| Garry P. Gippert,‡,⊥ Eva Thulin,‡ Johan Evenäs,‡,# L. Anders Svensson,§,▼ and Sara Linse*,‡

Departments of Physical Chemistry 2 and of Molecular Biophysics, P.O. Box 124, Lund University, SE-221 00 Lund, Sweden

Received March 16, 2001; Revised Manuscript Received June 4, 2001

ABSTRACT: Water molecules are found to complete the Ca^{2+} coordination sphere when a protein fails to provide enough ligating oxygens. Hydrogen bonding of these water molecules to the protein backbone or side chains may contribute favorably to the Ca^{2+} affinity, as suggested in an earlier study of two calbindin D_{9k} mutants [E60D and E60Q; Linse et al. (1994) *Biochemistry 33*, 12478−12486]. To investigate the generality of this conclusion, another side chain, Gln 22, which hydrogen bonds to a Ca^{2+}-coordinating water molecule in calbindin D_{9k}, was mutated. Two calbindin D_{9k} mutants, (Q22E+P43M) and (Q22N+P43M), were constructed to examine the interaction between Gln 22 and the water molecule in the C-terminal calcium binding site II. Shortening of the side chain, as in (Q22N+P43M), reduces the affinity of binding two calcium ions by a factor of 18 at low ionic strength, whereas introduction of a negative charge, as in (Q22E+P43M), leads to a 12-fold reduction. In 0.15 M KCl, a 7-fold reduction in affinity was observed for both mutants. The cooperativity of Ca^{2+} binding increases for (Q22E+P43M), while it decreases for (Q22N+P43M). The rates of Ca^{2+} dissociation are 5.5-fold higher for the double mutants than for P43M at low ionic strength. For both mutants, reduced strength of hydrogen bonding to calcium-coordinating water molecules is a likely explanation for the observed effects on Ca^{2+} affinity and dissociation. In the apo forms, the (Q22E+P43M) mutant has lower stability toward urea denaturation than (Q22N+P43M) and P43M. 2D ^{1}H NMR and crystallographic experiments suggest that the structure of (Q22E+P43M) and (Q22N+P43M) is unchanged relative to P43M, except for local perturbations in the loop regions.

Calcium binding proteins are involved in a large number of different physiological reactions taking place in all forms of life (i.e., flagella movement, intracellular signaling, the complement system, blood coagulation, muscle contraction, and neurotransmitter release in synapses), from prokaryotes to the advanced forms of multicellular eukaryotes (*1*). In each case, the calcium affinity is tuned to meet the requirements imposed by the particular protein function and by the ion concentration intervals in the cellular or extracellular environment. Among protein factors contributing to the affinity are the arrangement in sequence and the 3D structure of potential ligating oxygens, surface charges, preformation of the binding site in the Ca^{2+}-free state, conformational changes, etc. (*2*). However, it is hard to predict the calcium affinity of a particular protein. The affinity is a net balance of many different contributions stemming from the entire protein plus solvent, and the individual contributions may not be transparent.

For many proteins, the free energy of Ca^{2+} binding ($\Delta G^\circ = -RT \ln K$) is dominated by entropic contributions. A solvated calcium ion is irregularly coordinated by six to eight water molecules in its first hydration shell (*3, 4*). The release of these water molecules upon binding a calcium ion to a protein gives a large and favorable entropy contribution to ΔG. The more water is released, the higher is the entropy contribution to the affinity. However, to achieve an optimal coordination of the calcium ion in the site, one or more water molecules are often kept in the Ca^{2+}-coordinating sphere of a protein. It may not be possible to fold the protein chain to provide enough coordinating oxygen ligands by protein−calcium interactions alone. There could also be an advantage of having one or more water molecules in the binding site to facilitate the dynamics (uptake and release) of the ion(s). In addition, proteins have not evolved to have the highest possible Ca^{2+} affinity but to have suitable affinity and kinetics to function properly in their biological context. Keeping water molecules in the coordination sphere may be one way of avoiding an unsuitably high affinity.

The coordinating water molecules are seen in crystal structures of calcium binding proteins. In these structures,

† This work was supported by grants from the Swedish Natural Science Research Foundation (S.L.), the Lund Graduate School of Biomedical Research (stipend to J.F.), and the Swedish Foundation of Strategic Research (A.M.).

* Corresponding authors: jonas.fast@fkem2.lth.se, sara.linse@fkem2.lth.se, Phone + 46 46 222 83 42, Fax + 46 46 222 45 43.

‡ Department of Physical Chemistry 2.

§ Department of Molecular Biophysics.

|| Present address: Oxford Centre for Molecular Sciences, University of Oxford, New Chemistry Laboratory, South Parks Rd., Oxford OX1 3QT, England.

⊥ Present address: Structural Bioinformatics Advanced Technologies A\S, Agern Alle', DK-2970 Hørsholm, Denmark.

Present address: AstraZeneca, R&D Lund, Medicinal Chemistry, SE-221 87 Lund, Sweden.

▼ Present address: NovoNordisk A/S, Novo Alle', DK-2880, Bagsvaerd, Denmark.

10.1021/bi010551h CCC: $20.00
Published on Web 07/26/2001

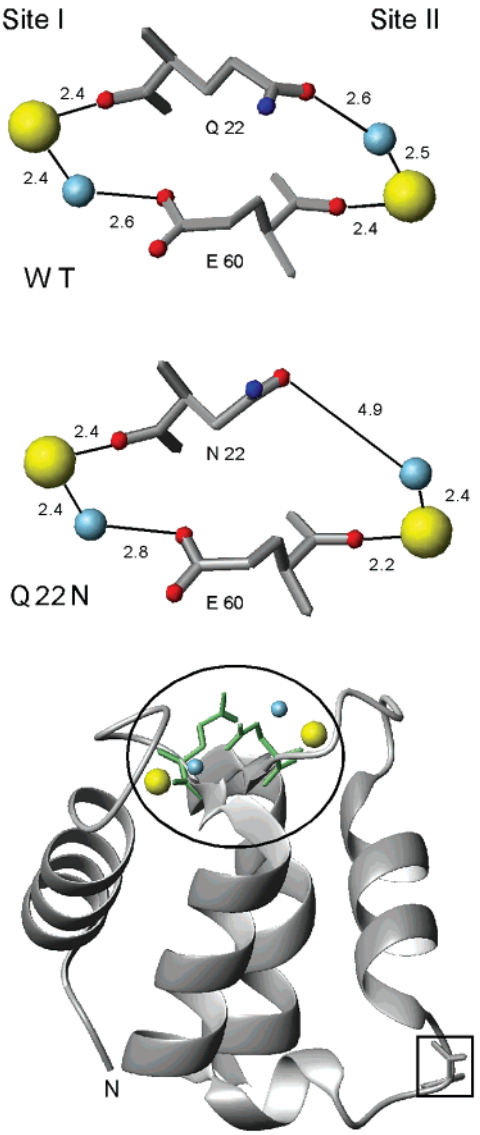

FIGURE 1: Symmetrical arrangement of Q22 and E60 of calbindin D_{9k} wild type (top) and of N22 and E60 in (Q22N+P43M) (middle). Crystallographic coordination distances are indicated. Large yellow spheres are calcium ions, and small blue spheres are water molecules. The complete wild-type protein is shown at the bottom with the circle indicating the location of Q/N22 and E60. The box indicates where the P43M mutation is located in the linker region. Figures were generated in MOLMOL (*36*) from PDB files 4ICB (WT) and 1HT9 [(Q22N+P43M)].

there are in general several potential hydrogen bond donors/acceptors at a suitable distance and angle from each Ca^{2+}-coordinating water molecule. Attempts to correlate the number and strength of such hydrogen bonds with the Ca^{2+} affinity are complicated by the fact that binding constants are mostly obtained as an effective mean value of several calcium sites and not explicitly for each calcium site of the protein. Furthermore, there are many interactions and factors, including the number of coordinating water molecules, which contribute to the affinity differences among calcium binding proteins. A more fruitful way to address the role of hydrogen bonds that stabilize coordinating water molecules may be through mutations that perturb such hydrogen bonds.

In calbindin D_{9k}, a small ($M_w = 8500$) globular protein of the calmodulin superfamily, there is one water molecule in each of the two EF-hand Ca^{2+} sites (Figure 1). The water molecule in the C-terminal site (site II, canonical EF-hand) is hydrogen bonded to the side chain oxygen of Gln 22.[1] The backbone carbonyl oxygen of Gln 22 coordinates the calcium ion in the N-terminal site (site I, pseudo-EF-hand). Another residue, Glu 60, is found in EF-hand loop II, in the homologous position of Gln 22. The side chain carboxylate oxygen of Glu 60 is hydrogen bonded to the water molecule in site I, while the backbone carbonyl oxygen coordinates the calcium ion in site II. Both Gln 22 and Glu 60 are located directly downstream of the short conserved two-strand β-sheet segment, which connects two EF-hand motifs through hydrogen bonds between residues Leu 23 and Val 61 (*5*).

The mutation Glu 60 → Asp, which shortens the side chain by one methylene carbon unit, reduces the total Ca^{2+} affinity and increases the cooperativity of Ca^{2+} binding (*6*). Another mutation, Glu 60 → Gln, which neutralizes the residue, results in reduced cooperativity and a very small reduction in total affinity (*7*). Through crystallographic studies of the mutants, it was suggested that the Glu 60 side chain contributes to the Ca^{2+} affinity by stabilizing the Ca^{2+}-coordinating water molecule (*6*). Henzl et al. (*8*) found that the calcium affinity of the CD site in oncomodulin decreases by a factor of 25 when Asn 59 is substituted with a glycine residue. Asn 59 hydrogen bonds to a water molecule that coordinates calcium, and the authors suggested that the mutation weakened the interaction of water with calcium.

The present work aims at understanding the role of the symmetric arrangement of Glu 60 and Gln 22 in calbindin D_{9k}, through mutagenesis of residue Gln 22. Two mutants were constructed; (Q22E+P43M) and (Q22N+P43M), changing the side chain charge and length, respectively. To address the specificity of charge effects, the N21D mutant with the neighboring Asn 21 → Asp substitution was produced. Several biophysical methods were used to examine the effects of the mutations. The change in Ca^{2+} affinity and cooperativity was studied by competition titrations in the presence of a chromophoric chelator. Ca^{2+} dissociation rates were measured using stopped-flow fluorescence. Circular dichroism was used to measure the stability toward urea denaturation. To establish whether conformational changes had occurred, 2D ^{1}H NMR spectra were collected and backbone proton chemical shifts were analyzed. Crystallographic data were obtained for (Q22N+P43M) and were used to explain effects in the Ca^{2+} binding sites.

MATERIALS AND METHODS

Proteins. Bovine calbindin D_{9k} wild type and mutants (Q22E+P43M), (Q22N+P43M), N21D, E60D, and E60Q

[1] Abbreviations: NMR, nuclear magnetic resonance; CD, circular dichroism; COSY, correlated spectroscopy; NOESY, nuclear Overhauser enhancement spectroscopy; TOCSY, total correlation spectroscopy; DIPSI, decoupling in the presence of scalar interactions; EDTA, ethylenediaminetetraacetic acid; EGTA, ethylene glycol bis(β-aminoethyl ether)-*N*,*N*,*N*′,*N*′-tetraacetic acid; DSS, 2,2-dimethyl-2-silapentane-5-sulfonic acid; quin 2, 2-[[2-[bis(carboxymethyl)amino]-5-methylphenoxy]methyl]-6-methoxy-8-[bis(carboxymethyl)amino]quinoline; SDS−PAGE, sodium dodecyl sulfate−polyacrylamide gel electrophoresis; PDB, protein data bank; amino acids are denoted by their standard one- and three-letter codes; P43M, calbindin D_{9k} mutant with the substitution Pro 43 → Met; (Q22E+P43M), calbindin D_{9k} double mutant with the substitutions Gln 22 → Glu and Pro 43 → Met; (Q22N+P43M), calbindin D_{9k} double mutant with the substitutions Gln 22 → Asn and Pro 43 → Met.

as well as P43M were expressed in *E. coli* and purified as described previously (*9*). The purity and calcium content were confirmed by agarose gel electrophoresis in the presence of 1 mM EDTA or 2 mM $CaCl_2$, SDS−PAGE, isoelectric focusing, and ^1H NMR. The reference protein, P43M, is the minor-A form of bovine calbindin D_{9k} with two modifications. First, a methionine residue is attached to the N-terminus for expression purposes. Second, a P43M mutation is incorporated to eliminate multiple native forms due to cis/trans isomerization of the G42−P43 peptide bond as described previously (*10*). (Q22E+P43M) and (Q22N+P43M) contain methionine residues in positions 0 and 43. The N21D, E60D, and E60Q mutants do not contain the P43M substitution.

Chemicals. The chromophoric chelator quin 2 was obtained from Fluka Chemie AG, Buchs, Switzerland. Denaturation experiments were performed using ultrapure urea (BDH Chemicals Ltd., Poole, England). To produce Ca^{2+}-free buffers, membrane tubing (MW cutoff 3500; Spectrum Medical Industries Inc., Los Angeles, CA; boiled 4 times in doubly distilled water before use) was filled with 10 mL of Chelex 100 (BioRad, Richmond, CA), sealed, and stored in the solutions to absorb Ca^{2+}. Other chemicals were of the highest obtainable laboratory quality.

Chelator Method. To study the Ca^{2+} association and cooperativity of binding, each protein was titrated with calcium in the presence of a chromophoric chelator, quin 2, for which the absorbance at 263 nm decreases (approximately 85%) upon Ca^{2+} binding. The exact concentration of the chelator solution (in the range of 25−30 μM) was calculated from the absorbance at 239.5 nm in the presence of excess calcium (using $\epsilon_{239.5} = 4.2 \times 10^4$ L mol^{-1} cm^{-1} for quin 2). Lyophilized protein was dissolved in calcium-free (<1 μM Ca^{2+}) chelator solution to obtain a concentration of 25−30 μM. The absorbance at 263 nm (A_{263}) was recorded for the protein/chelator solution on a UV/Vis 920 spectrophotometer (GBC Scientific Equipment Pty Ltd., Victoria, Australia). Calcium solution (3 mM Ca^{2+} in 2 mM Tris-HCl, pH 7.5, with or without 0.15 M KCl) was added in portions of 4 μL. A_{263} was recorded after each calcium addition. The titration was continued until no absorbance change was seen for the last five additions. Larger additions (4 μL of 10 mM Ca^{2+} in 2 mM Tris-HCl, pH 7.5, with 0.15 M KCl) were made at the end of the titrations of the proteins in 0.15 M KCl.

The data analysis consists of computer fitting directly to the measured quantity: absorbance versus total calcium concentration. The initial calcium concentration and the dilution effect of the calcium additions were taken into account in the fits. The theoretical absorbance values at all data points were calculated for each set of trial parameters, and these were compared to the measured absorbance to calculate the sum of residuals, χ^2, which was minimized in an iterative procedure [see (*7*)]. The optimized parameters were K_1, K_2, F, A_{max}, and A_{min}. K_1 and K_2 are the macroscopic binding constants referring to the binding of the first and second calcium ion to the protein irrespective of what site is occupied in the protein (Figure 2). F is the protein concentration correction factor accounting for residual water in the lyophilized protein. A_{max} is the absorbance in calcium-free solution. A_{min} is the absorbance in calcium-loaded solution versus the total calcium concentration. For comparison of the mutants, the measured and the calculated absorbance and the total calcium concentrations were normalized. The total calcium concentration is normalized so that 1.0 corresponds to 1 times the chelator concentration plus 2 times the protein concentration.

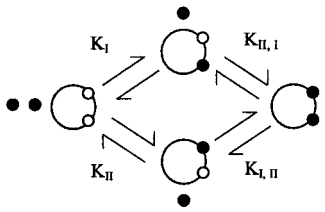

$$P + Ca^{2+} \xleftrightarrow{K_1} P \cdot Ca \qquad P \cdot Ca + Ca^{2+} \xleftrightarrow{K_2} P \cdot Ca_2$$

FIGURE 2: Definitions of macroscopic (K_1 and K_2) and microscopic (K_I, K_{II}, $K_{I,II}$, and K_{II}) calcium binding constants. $K_I = K_I + K_{II}$; $K_2 = K_{I,\,II}/(K_{II}/K_I)$.

Stopped Flow. To measure the dissociation of Ca^{2+} from calbindin D_{9k}, a chelator (21.2 μM quin 2), which changes optical properties upon Ca^{2+} binding, was mixed stepwise with the buffer and the Ca^{2+}-loaded protein solution in the stopped-flow equipment at an effective ratio of 1:10 (25 μL of buffer, 250 μL of chelator, and 25 μL of protein/Ca^{2+} solution, the dead volume of the tubing explaining the lower than expected effective ratio). As the reaction of Ca^{2+} with quin 2 is several orders of magnitude faster than the dissociation of Ca^{2+} from the protein (*11*), the time course of Ca^{2+} binding to the chelator reflects the Ca^{2+} dissociation from the protein. All solutions were made in 2 mM Tris-HCl, pH 7.5. The lyophilized proteins were dissolved to a concentration of 15 μM with 40 μM $CaCl_2$. The stopped-flow experiments were performed at 26 °C connected to a Biologic MOS-200 optical system as light source. The light was led to the cuvette through an optical fiber (Fiberguides Industries). The total fluorescence from excitation at 339 nm was detected by a Hamamatsu R-376 photomultiplier connected to a Biologic PMS200 photomultiplier detection unit. A 2 × 2 mm quartz cuvette was used, and a cutoff filter blocking transmission below 400 nm was inserted in front of the photomultiplier. Data sampling and equipment handling were performed by software from Bio-Kine. The stopped-flow data were analyzed with the software Kaleidagraph (Synergy Software) for Macintosh and fitted to the equation:

$$y = A_0 \cdot e^{-k^{off} \cdot t} + A_1 \qquad (1)$$

where k_{off} is the Ca^{2+} dissociation rate constant, A_0 is the amplitude, and A_1 is the fluorescence signal at t_∞.

Urea Denaturation and Circular Dichroism (CD). A set of samples with urea concentrations ranging from 0 to 9.5 M were prepared by mixing appropriate amounts of protein stock and two solutions containing 10 mM KH_2PO_4/KOH, 0.5 mM EGTA, pH 7.0, and either 0 or 10 M urea. Urea denaturation profiles of the apo forms of the proteins were obtained by recording the ellipticity at 222 nm and 25.1 °C on a Jasco-720 spectropolariometer, using a 2 mm quartz cuvette. The CD data were analyzed with the software Kaleidagraph (Synergy Software) for Macintosh and fitted to a linear extrapolation model assuming two-state unfolding as follows. The baselines before, Y_N, and after, Y_U, the actual

unfolding were assumed to be straight lines:

$$Y_N = k_N \cdot [D] + b_N \quad (2)$$

$$Y_U = k_U \cdot [D] + b_U \quad (3)$$

where k_N and k_U are the slopes, b_N and b_U are the intercepts, and [D] is the denaturant concentration. The observed ellipticity, Y_o, was fitted using the equation:

$$Y_o = \frac{(k_N \cdot [D] + b_N) + (k_U \cdot [D] + b_U) \cdot e^{-(\Delta G_{NU}(H_2O) - m_D[D])/RT}}{1 + e^{-(\Delta G_{NU}(H_2O) - m_D[D])/RT}} \quad (4)$$

where $\Delta G_{NU}(H_2O)$ is the unfolding free energy in pure water, m_D is the influence of denaturant concentration on the stability, R is the molar gas constant, and T is the temperature. The free energy toward unfolding by urea, ΔG_{NU}, is assumed to obey the linear equation:

$$\Delta G_{NU} = \Delta G_{NU}(H_2O) - m_D \cdot [D] \quad (5)$$

$[D] = C_m$, the urea concentration at the transition midpoint, when ΔG_{NU} is zero.

The errors in the reported values of the different parameters were estimated to one standard deviation. The standard deviations were obtained directly from the fitting procedures.

For presentation and comparison, the data were normalized according to

$$F_{app} = (Y_0 - Y_N)/(Y_0 - Y_U) \quad (6)$$

Y_0, Y_N, and Y_U are defined above. The normalized curve fit was calculated as

$$F_{app} = \frac{e^{-(\Delta G_{NU}(H_2O) - m_D[D])/RT}}{1 + e^{-(\Delta G_{NU}(H_2O) - m_D[D])/RT}} \quad (7)$$

^{1}H NMR Spectroscopy. 2D ^{1}H NMR spectra [COSY (*12*), TOCSY (*13*) [80 ms mixing time using a DIPSI-2 sequence (*14*)], and NOESY (*15*) [200 ms mixing time]) were recorded with 4096 and 1024 points in the direct and indirect dimension, respectively, on a Varian UNITY INOVA 600 NMR spectrometer with a proton frequency of 599.89 MHz at 27 °C. The Ca^{2+} forms of the proteins were dissolved to 4 mM in doubly distilled H_2O with 10% D_2O and 1 extra equiv of $CaCl_2$ at pH 6.01. ^{1}H chemical shifts were referenced to DSS at 0.00 ppm. The spectra were processed using the FELIX 98 software package (Molecular Simulations Inc.). FELIX 98 was used together with the software GENXPK (*16*) in the assignment of the mutants, with the reported assignment of P43M as a reference (*17*). The chemical shifts of the mutated residues were corrected for differences in the random coil chemical shifts of glutamine, glutamic acid, and asparagine (*18*).

RESULTS

Macroscopic Calcium Binding Constants. Each protein [P43M, (Q22E+P43M), (Q22N+P43M), and N21D] was titrated with Ca^{2+} in the presence of the chromophoric chelator quin 2. Normalized data at low salt concentration are shown in Figure 3, and the results at physiological (0.15 M) and low (no added) KCl concentrations are listed in Table 1. At low ionic strength, the total affinity of binding two calcium ions (i.e., the product of the two macroscopic binding constants, K_1K_2) in (Q22E+P43M) and (Q22N+P43M) decreases by a factor of 12 and 18, respectively, in comparison with P43M. This corresponds to an increase of 6.3 and 7.3 kJ mol^{-1} for (Q22E+P43M) and (Q22N+P43M), respectively, in ΔG_{tot}, the free energy of binding two calcium ions [$\Delta G_{tot} = -RT \ln(K_1K_2)$]. N21D has 2 kJ mol^{-1} higher total affinity than the wild type at low salt concentration (98 and 96 kJ mol^{-1}, respectively). At physiological ionic strength, the Ca^{2+} affinity for both (Q22E+P43M) and (Q22N+P43M) is a factor of 7 lower than in P43M, and ΔG_{tot} increases by approximately 4.7 kJ mol^{-1}. The total affinity for N21D is comparable to that of the wild type at physiological ionic strength.

Effects on the cooperativity can be estimated through the parameter $-\Delta\Delta G_{\eta=1} = RT \ln(4K_2/K_1)$, which is the lower limit to $-\Delta\Delta G = RT \ln(K_{I,II}/K_I)$, the free energy of

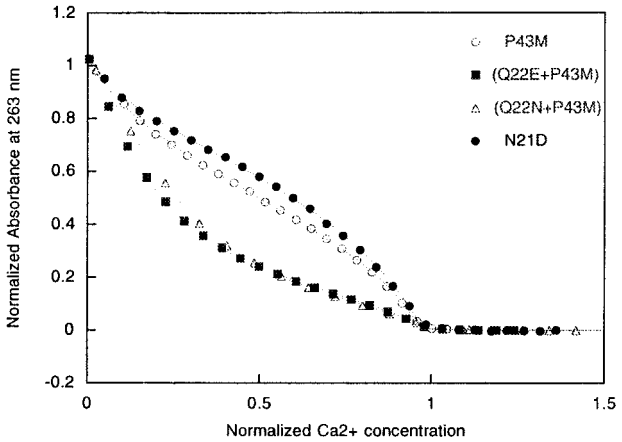

FIGURE 3: Ca^{2+} titrations of quin 2 in the presence of P43M (○), N21D (●), (Q22E+P43M) (■), and (Q22N+P43M) (△) at low ionic strength. Normalized absorbance at 263 nm as a function of normalized total Ca^{2+} concentration. The lines are curves obtained by least-squares fitting to the data points as described (*7*). The total Ca^{2+} concentration is normalized so that 1.0 corresponds to 1 times the chelator concentration plus 2 times the protein concentration.

Table 1: Ca^{2+} Binding Parameters[a]

protein	[KCl] (M)	log K_1	log K_2	$-\Delta\Delta G_{\eta=1}$ (kJ mol^{-1})	ΔG_{tot} (kJ mol^{-1})
P43M[b]	–	7.8	8.6	8.2	−93.3
P43M[b]	0.15	6.0	6.5	6.4	−71.4
(Q22E+P43M)	–	7.1	8.1	9.0	−87.0
(Q22E+P43M)	0.15	5.2	6.5	11.0	−66.4
(Q22N+P43M)	–	7.2	7.9	7.2	−86.0
(Q22N+P43M)	0.15	5.8	5.8	3.4	−66.5
wild type[c]	–	8.2	8.6	6.9	−96.2
wild type[c]	0.15	6.3	6.5	5.5	−73.4
E60Q[d]	–	8.0	8.5	6.1	−94.4
E60Q[d]	0.15	6.6	6.2	1.6	−73.3
E60D[d]	–	6.9	8.4	12.0	−87.2
E60D[d]	0.15	5.4	6.5	10.0	−68.3
N21D	–	7.9	8.8	8.2	−95.4
N21D	0.15	5.8	7.0	10.4	−72.6

[a] Macroscopic Ca^{2+} binding constants, K_1 and K_2; free energy of binding two calcium ions, $\Delta G_{tot} = -RT \ln(K_1K_2)$; a lower limit to the free energy of interaction between the two sites, $-\Delta\Delta G_{\eta=1} = RT \ln(4K_2/K_1)$. Mean values for two experiments are shown. [b] Data from Linse et al., 1993 (*34*). [c] Data from Linse et al., 1991 (*7*). [d] Data from Linse et al., 1994 (*6*).

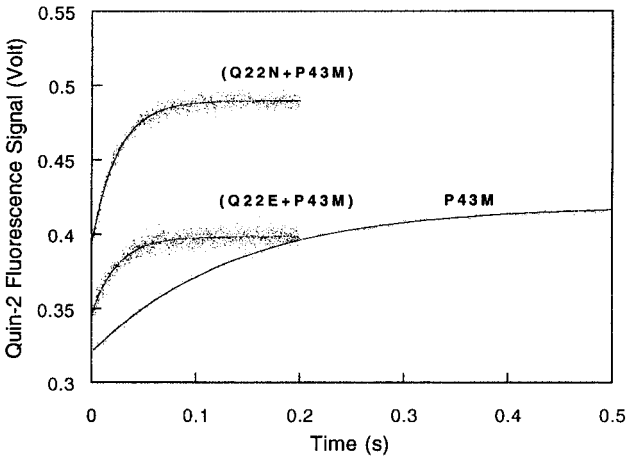

FIGURE 4: Stopped-flow fluorescence kinetic traces for P43M, (Q22E+P43M), and (Q22N+P43M) together with fitted curves using single-exponential functions.

Table 2: Dissociation Rate Constant, k^{off}, Obtained from the Fitting of Stopped-Flow Data, and the Association Rate Constant for the Second Bound Calcium, k^{on}, Based on K_2[a]

protein	K_1K_2 (M^{-2} s^{-2})	k^{off} (s^{-1})	k^{on} (s^{-1})[b]
P43M	2.2×10^{16}	7.3	2.8×10^9
(Q22E+P43M)	1.8×10^{15}	40.8 ± 0.4	5.2×10^9
(Q22N+P43M)	1.2×10^{15}	40.9 ± 0.9	3.0×10^9
wild type	6.3×10^{16}	5.3	$\geq 2.1 \times 10^9$
E60D	2.0×10^{15}	11.3	2.8×10^9
E60Q	3.2×10^{15}	2.5	0.8×10^9

[a] Errors are less than 0.1, unless indicated. [b] Based on K_2.

interaction between the sites (*7*). Since $-\Delta\Delta G_{\eta=1}$ is a function of the ratio of the two macroscopic binding constants, it is inherently difficult to determine with high precision, and the uncertainty becomes larger with increasing $-\Delta\Delta G_{\eta=1}$. When $-\Delta\Delta G_{\eta=1}$ is close to 10 kJ mol^{-1} or above, the shape of the titration curve changes very little even with a rather large increase in $-\Delta\Delta G_{\eta=1}$. Hence, only the effects seen at 0.15 M KCl can be considered significant between mutants and P43M. Under this condition, there is an apparent increase in the cooperativity ($-\Delta\Delta G_{\eta=1}$) due to the charge introduction; from 6.4 to 11 kJ mol^{-1} for (Q22E+P43M) compared to P43M. For (Q22N+P43M), there is instead a decrease to 3.4 kJ mol^{-1}. At low salt concentration, the difference between $-\Delta\Delta G_{\eta=1}$ of (Q22N+P43M) and (Q22E+P43M) is significant, with higher positive cooperativity for Q22E, and is evident from a visual inspection of the titration curves (Figure 3).

Ca^{2+} Dissociation Rates by Stopped-Flow Fluorescence. Stopped-flow studies were carried out for the wild-type protein and for the mutants, P43M, (Q22E+P43M), (Q22N+P43M), E60D, and E60Q, to obtain accurate values of the Ca^{2+} dissociation rates. The E60D and E60Q mutants have a proline in position 43 as in the wild-type protein, while (Q22E+P43M) and (Q22N+P43M) contain the additional Pro43 → Met substitution as in P43M, and the latter mutant is used as a point of reference for (Q22E+P43M) and (Q22N+P43M). Examples of the data are shown in Figure 4 and the results are summarized in Table 2. Both mutants (Q22E+P43M) and (Q22N+P43M) have a 5.5-fold increase in dissociation rate compared to P43M. E60D shows approximately twice the rate of the wild type, whereas E60Q has half the dissociation rate of the wild type. P43M has a slightly higher dissociation rate constant than the wild type.

Table 3: Stability Parameters of the Apo Forms of the Calbindin D_{9k} Mutants[a]

protein	$\Delta G_{NU}(H_2O)$ (kJ mol^{-1})	m_D (kJ mol^{-1})	C_m (M)
P43M	23.4 ± 0.9	-4.15 ± 0.15	5.60 ± 0.29
(Q22E+P43M)	15.5 ± 0.4	-3.65 ± 0.09	4.25 ± 0.16
(Q22N+P43M)	16.8 ± 0.3	-3.71 ± 0.06	4.53 ± 0.12
N21D[b]	20.6 ± 0.3	-3.89 ± 0.06	5.28 ± 0.11

[a] $\Delta G_{NU}(H_2O)$ is the free energy of unfolding in the absence of denaturant, m_D is the influence of the denaturant concentration on the stability, and C_m is the urea concentration of half-denaturation. [b] N21D does not contain the P43M mutation and is compared to the wild type with a $\Delta G_{NU}(H_2O)$ of 25 kJ mol^{-1}.

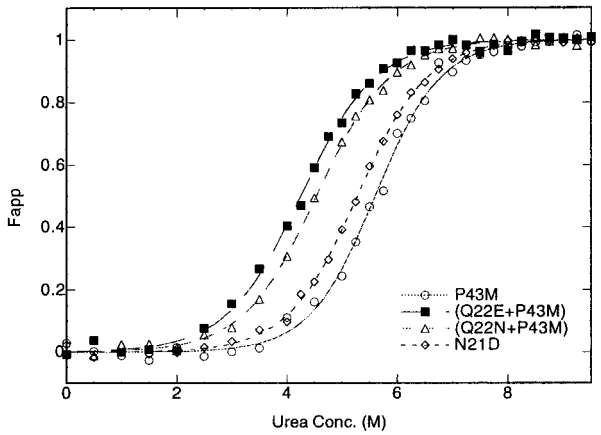

FIGURE 5: Urea denaturation profiles for the apo forms of P43M (○), N21D (●), (Q22E+P43M) (■), and (Q22N+P43M) (△). Normalized ellipticity, F_{app}, at 222 nm as a function of urea concentration.

Stability Effects by Urea Denaturation. Urea denaturations were monitored by CD spectroscopy to study stability effects of the mutations. The free energies of unfolding in the absence of denaturant, $\Delta G_{NU}(H_2O)$, the influence of denaturant concentration on the stability, m_D, and the urea concentrations at the transition midpoint, C_m, were obtained by fitting to the observed ellipticity at 222 nm as a function of urea concentration for solutions of calbindin D_{9k} mutants as described under Materials and Methods. The results are summarized in Table 3. To enable a visual comparison of the proteins, the normalized ellipticity, F_{app}, as a function of urea concentration is shown in Figure 5. P43M shows a $\Delta G_{NU}(H_2O)$ of 23.4 kJ mol^{-1}. $\Delta G_{NU}(H_2O)$ values for (Q22E+P43M), (Q22N+P43M), and N21D decrease by 7.9, 6.6, and 2.8 kJ mol^{-1}, respectively. (Q22E+P43M) has the lowest C_m followed by (Q22N+P43M), N21D, and P43M. The m_D values show that the denaturant concentration affects the mutants slightly less than P43M.

2D ^1H NMR Assignments. The ^1H assignments of the mutants (Q22N+P43M) and (Q22E+P43M) are compared to those of the P43M mutant. The P43M mutant has earlier been shown to have similar structure, and similar chemical shifts, as wild-type calbindin D_{9k} (*17*, *19*−*21*). The chemical shift assignments of (Q22E+P43M) and (Q22N+P43M) were accomplished using TOCSY and NOESY spectra in an "assignment by comparison" strategy. The assignments were continuously cross-checked using NOESY spectra to verify the backbone connectivities. A chemical shift differ-

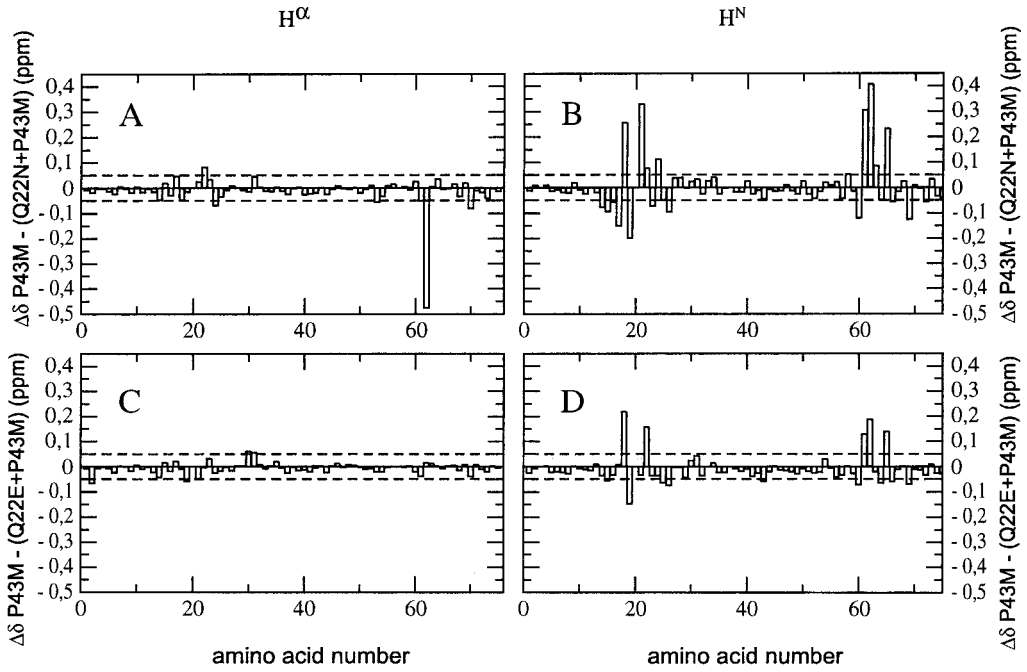

FIGURE 6: Δδ(ppm), the difference in chemical shift between P43M and double mutant, is shown for (A) H^{α}(P43M−(Q22N+P43M)), (B) H^{N}(P43M−(Q22N+P43M)), (C) H^{α}(P43M−(Q22E+P43M)), and (D) H^{N}(P43M−(Q22E+P43M)). There are prolines at positions 3, 20, and 37.

ence of ±0.05 ppm or more between P43M and a mutant is considered significant. In general, both (Q22N+P43M) and (Q22E+P43M) have chemical shifts very close to those of P43M, and differ only in the loop regions. All observed shift changes are below 0.5 ppm. For (Q22E+P43M), the most pronounced H^{N} shifts changes are seen for Gly 18, Asp 19, and Glu 22 itself (taking the random coil shifts into account) in site I, as well as Val 61, Ser 62, and Glu 65 in site II (Figure 6D). Small, but significant H^{α} shift changes are found for Asp 19, Leu 30, and Leu 30 (Figure 6C). There are more H^{N} resonances with pronounced shift changes in the spectrum of (Q22N+P43M), and the largest shift differences are seen mainly in the same residues as in (Q22E+P43M) (Figure 6B). There are significant H^{α} shift changes for residues Asn 22, Ser 24, and Ser 62. Ser 62 exhibits the largest H^{N} and H^{α} shift change in (Q22N+P43M) and the second largest H^{N} shift change in (Q22E+P43M).

X-ray Crystallography. The crystal structure of the double mutant (Q22N+P43M) has been determined to 1.75 Å resolution. The high resolution makes it possible to estimate the positions of individual atoms with an accuracy of 0.1−0.2 Å according to a Luzzatti plot (*22*). Only small changes are observed at the site of the Gln 22 → Asn substitution (Figure 1). The hydrogen bond between Gln 22 and the calcium-coordinating water in EF-2 site II (2.6 Å) is lost when Asn 22 is introduced (equivalent distance of 5.0 Å). Some stabilization of this water is still possible, though. The water molecule makes a hydrogen bond to Asp 58 OD1 in the same EF-hand loop, both in wild-type calbindin D_{9k} (3.2 Å) and in Q22N (2.9 Å). Another interesting observation in (Q22N+P43M) is one weaker (2.9 Å) and one stronger (2.7 Å) hydrogen bond in the small β-sheet connecting the EF-hand loops. The water in site I is stabilized by the carboxyl group of Glu 60 as in the wild-type protein; however, the hydrogen bond is around 0.15 Å longer (2.85 Å). This movement is connected to the movement of the carbonyl oxygen of Glu 60, which moves 0.15 Å closer to the calcium ion in site II. The distance between the calcium ion and the water molecule in site II is marginally shortened (by 0.15 Å), and the calcium ion distance to the carbonyl oxygen of Glu 60 is shortened by 0.16 Å. These changes are basically within the experimental error range. The length of the hydrogen bond between Gln H^{ϵ} 22/Asn H^{δ} 22 and the water molecule (site I) is increased by 0.20 Å, and the water molecule has moved marginally closer to the calcium ion (0.09 Å). The carbonyl oxygen coordination distance from Asn 22 to the calcium ion has not changed, but the coordination angle could very well have changed since the calcium ion has moved 0.28 Å compared to the crystal structure of P43M.

DISCUSSION

Before evaluating the effects of the mutations on biophysical properties, it is important to establish that no major changes in protein structure are introduced, e.g., by X-ray crystallography and NMR spectroscopy. To our surprise, (Q22N+P43M) crystallizes as a 3D (sub)domain-swapped dimeric structure in which the EF-hand I from one chain pairs with EF-hand II from another chain, and vice versa. The main features of this structure, which was obtained at pH 5, are reported elsewhere (*23*). However, gel filtration and NMR line widths suggest that the protein is monomeric at pH 6 (the conditions of the present NMR assignments) and at pH 7−7.5 (the conditions of the biophysical studies). The crystal structure for (Q22N+P43M) reveals that the fold of each domain comprising EF-hands I and II is strictly conserved, and that there are small but significant structural effects only in the loop region. Hence, structural effects seen within each domain of the swapped dimer are likely to represent perturbations due to the Gln22 → Asn substitution. These effects will be discussed in relation to the observed effects on Ca^{2+} binding properties and stability.

The general conclusion from comparison of the ^1H backbone chemical shifts is that there are no major structural changes in (Q22E+P43M) and (Q22N+P43M). The chemical shift differences are smaller between (Q22E+P43M) and P43M than between (Q22N+P43M) and P43M, especially for H^α, and all chemical shift effects are below 0.5 ppm. H^N shifts are more sensitive than H^α to the surrounding environment, and differences between the H^N shifts of our mutants and those of P43M are found primarily in the loop regions where we expect to observe shift changes due to local structural differences introduced by the mutations. Residue 22 and Glu 60 are close together in space, and mutation of residue 22 may influence the chemical shifts of Glu 60 and vice versa. In the previous study, the E60D mutant exhibited the largest shift differences compared with P43M for Gln 22 (*6*). In the present study of (Q22E+P43M) and (Q22N+P43M), the H^N shift of E60 is among the most affected shifts.

Based on the crystal structure of (Q22N+P43M), the shift differences of the residues around site II arise as a consequence of the differences in the chemical environment and not from significant structural changes in the residues themselves. The shift changes seen in some residues of (Q22E+P43M) are likely to come from changes in the electrostatic environment and differences in water coordination. The shortening of the side chain of residue 22 and the movement of the water molecule disrupt the hydrogen bond to the water molecule and are expected to give rise to shift differences for the side chain amide protons of residue 22, but are not a likely source for the changes in the backbone H^α and H^N shift changes. The crystallographic studies show that the side chain of residue 22 has moved considerably relative to the amide proton of Asn 21, but it is too far away from the H^α to have any influence. The chemical shift data are consistent with this, since the second largest shift change observed in (Q22N+P43M) is the H^N shift of Asn 21, but no significant H^α shift change is seen for this residue. The same effect could be used to explain the third largest shift, H^N of Val 61, which has the same character as Asn 21 (large H^N shift change and no, or a minor, H^α shift change). The large H^N shift change of Glu 65, whose bidentate carboxyl group coordinates the calcium ion in site II, could be explained by the difference in coordination geometry of the calcium ion in site II caused by the mutation. The largest shift difference is observed for Ser 62 H^α in (Q22N+P43M). The hydroxyl side chain of Ser 62 hydrogen bonds to the bidentate carboxyl group of Glu 65. The H^β shifts of Ser 62 are unperturbed, so the changes in the side chain environment will probably not explain the shift change of the H^α. The C^α of Ser 62 is in the vicinity of the side chain of Gln 22 in the wild type and P43M. The mutation Gln 22 → Asn increases this distance due to the shortened side chain and side chain movement. This alters the chemical environment for Ser 62 H^α, and may explain the shift difference. The H^α shift of Ser 62 is not affected in (Q22E+P43M) but is largely downfield shifted in (Q22N+P43M). The H^N shift is upfield shifted to the same extent in both mutants. An increased chemical shift, e.g., downfield shifted, speaks for a smaller shielding effect from the external magnetic field due to the surroundings deshielding the H^α of Ser 62. The side chain withdrawal may be the deshielding factor. On the other hand, there seems to be an increased shielding experienced by the H^N of Ser 62. H^N is directed into site II and may probe the changes there by a decreased chemical shift.

Affinity. The decreased affinity for calcium for both mutants is explained by a weakened or disrupted hydrogen bond to the coordinating water molecule in site II. In (Q22N+P43M), this is an effect from the shortened side chain that is too far away to make a hydrogen bond to the water molecule in site II. In (Q22E+P43M), a repulsion effect is likely to lead to a weakening in the water coordination.

Both the removal (as in E60Q) and addition [as in (Q22E+P43M)] of a negative charge lead to a decreased affinity, despite the opposite nature of the alteration. In the charge control mutant, N21D, the addition of a surface charge seems to decrease the affinity marginally. The Asn 21 side chain is directed toward the solution and is not involved in the coordination of the calcium ion. An increase in affinity would be expected based on other studies of mutated surface charges (*7*). The lack of such an effect may suggest that too much negative charge is counterproductive as it leads to destabilizing electrostatic repulsion between the EF-hands. In any case, the significantly reduced Ca^{2+} affinity for (Q22E+P43M) cannot be explained as a surface charge effect and therefore must have a more intricate structural reason. The area around the binding sites is highly negatively charged, and the charged Glu 22 may be repelled from this area, thereby weakening the hydrogen bond to the water molecule in site II. A repulsion between the introduced Glu 22 and the Glu 60 that is near is supported by the significant shift change seen for these two residues in the NMR spectra of (Q22E+P43M).

Side chain shortening by one methylene carbon unit was found to decrease the affinity both in E60D and in (Q22N+P43M). The hydrogen bonding distances to the Ca^{2+}-coordinating water molecules from Asp 60 (site I) and Gln 22 (site II) are increased in the crystal structure of E60D compared to the wild type (*6*). The present crystal structure for (Q22N+P43M) shows that the hydrogen bond between the water ligand in site II and residue 22 is disrupted with a distance increase of 2.3 Å. The increased distance to N22 probably makes the water ligand more labile, which would destabilize the calcium coordination and could explain the decreased calcium affinity of site II. There is no structural movement of the side chain of Glu 60 of (Q22N+P43M) compared to the crystal structure of P43M, but Glu 60 is protonated at pH 5 (Kesvatera et al., personal communication), which suggests that its position in the (Q22N+P43M) crystal structure is not representative for the conditions of the calcium binding studies (pH 7.5). The H^N shift of Asn 22 is affected via the carbonyl oxygen atom itself when the calcium ion changes position in site I. These minor changes, compared to site II, may together explain the decreased affinity of calcium binding to site I, and the shift changes of the backbone amide protons.

Cooperativity. In (Q22E+P43M), the addition of a negative charge leads to enhanced positive cooperativity compared to P43M, while the opposite effect is seen for (Q22N+P43M).

Cooperative Ca^{2+} binding is observed for a number of highly negatively charged systems, e.g., the γ-carboxyglutamic acid-rich modules (Gla-modules) of the blood coagulation factors (*24*). In such a system, there is an all-

or-nothing effect leading to high cooperativity. The charges are far apart in the apo state, and bringing them close together as in the fully calcium loaded state is electrostaticly unfavorable, unless all calcium ions are bound. Calbindin D_{9k} carries a large proportion of negatively charged groups in and around the Ca^{2+} binding sites, and a significant reduction of the positive cooperativity has been observed for mutants for which the negative charge in position 17, 19, or 60 has been removed (*7*). The increased cooperativity upon addition of a negative charge [as in (Q22E+P43M)] is in line with these earlier findings. The role of charged residues in the cooperativity is likely to be similar to that in Gla modules although the conformational change is much smaller. In the apo state of calbindin D_{9k}, the negative charges of the two empty Ca^{2+} binding sites repel each other and are further apart than in the Ca_2 state. Binding of the first calcium ion may bring the charged groups closer together in the binding site area, enhancing the attraction of the second calcium ion. The introduction of additional negative charges would enhance this effect, which we can see in the increased cooperativity of (Q22E+P43M), while a less charged system would have reduced cooperativity as indeed observed for E60Q and other earlier mutants (*6*, *7*). Similarly, addition of salt, which screens the electrostatic interactions, leads to reduced cooperativity (*6*, *7*, *25*). The repulsion between the introduced Glu 22 and the nearby Glu 60 is observed as significant shift changes seen for these two residues in the NMR spectrum of (Q22E+P43M) compared to the P43M spectrum.

The positive cooperativity of Ca^{2+} binding is a net balance of several factors, including electrostatic interactions, working for or against cooperativity. One effect promoting cooperativity is the larger changes in structure and dynamics, which take place on binding the first compared to the second calcium ion (*26*−*28*). Also the β-sheet connecting the loops has been suggested to be important for the cooperativity (*29*, *30*). Val 61 and Leu 23 make two hydrogen bonds with each other in this short two-stranded β-sheet. The hydrogen bond between Val 61 O and Leu 23 N is situated next to the substitution, and is indeed weakened in (Q22N+P43M). Possibly, the missing hydrogen bond between the Asn 22 side chain and the water in site II destabilizes the β-sheet connecting the EF-hands. This is in agreement with a previous observation of the sheet in Mg^{2+}-loaded calbindin D_{9k}. In this structure, a weakening of both hydrogen bonds making up the small β-sheet is observed, and both the Gln 22 and the Glu 60 side chains have lost their hydrogen bonds to the water molecules in the opposite EF-hand (*31*).

In the crystal structure of (Q22N+P43M), the intramolecular distance between Val 61 O and Leu 23 N is significantly shorter than the distance between Val 61 N and Leu 23 O. The H^N shift of Val 61 is significantly upfield shifted in both mutants whereas Leu 23 is only slightly downfield shifted. A disturbed water molecule coordination in (Q22N+P43M) and a repulsion effect between Glu 22 and Glu 60 in (Q22E+P43M), as well as a possible disturbed water molecule coordination, may be the factors that affect the shifts in the β-sheet region of both mutants. It could explain a weakened hydrogen bond network between Val 61 and Leu 23, which may then explain the decreased cooperativity seen in (Q22N+P43M). However, in (Q22E+P43M), the charge effects are probably larger than the opposing β-sheet effects and this facilitate an increased cooperativity.

Rate Constants. For both mutants, the reduced affinity is explained by increased dissociation rate constants, while there is little effect on the association rate constants. The disrupted or weakened hydrogen bond to the calcium-coordinating water molecule results in a higher calcium release rate.

The association rate constant (k^{on}) for the second bound calcium ion can be estimated from the equilibrium constant K_2 and the dissociation rate constant (k^{off}) as $K_2 \times k^{off}$ (Table 2), if we assume that the release of the first calcium ion is rate-limiting (the second bound corresponds to the first released). These estimates of k^{on} showed a slight (2-fold) increase for (Q22E+P43M) compared to P43M, which may be explained by the increased negative surface charge which will facilitate attraction of calcium ions from the surrounding solution (*32*). More significant, k^{off} increases 6-fold for both (Q22E+P43M) and (Q22N+P43M), suggesting that the reduced Ca^{2+} affinity in both mutants originates from a decreased stability of the calcium ion in the site. In case of (Q22N+P43M), the shortened side chain may not reach close enough to the water molecule for strong hydrogen bonding. In the case of (Q22E+P43M), the introduced negative charge may limit the strength of the hydrogen bond because of electrostatic repulsion between E22 and the Ca^{2+} ligands in site II. Although for both position 60 mutants the Ca^{2+} dissociation rate is less affected than for the position 22 mutants, the observed effects can be explained along the same lines. A decreased stability of the Ca^{2+} ion in the site can be inferred for E60D (increased off-rate), for which the crystal structure shows a longer and weaker hydrogen bond between the side chain carboxylate and the Ca^{2+}-coordinating water molecule (*6*). On the contrary, an increased stability of the Ca^{2+} ion in the site can be inferred for E60Q (reduced off-rate), which may suggest a strengthened hydrogen bond to the water molecule. The uncharged glutamine side chain does not experience any electrostatic repulsion by the negatively charged residues in site I, and may therefore interact more tightly with the water molecule in this site than does the glutamic acid in the wild type. However, the reduced negative surface charge leads to a 3−4-fold lower Ca^{2+} on-rate in E60Q compared to the wild type, and the net balance is a reduced Ca^{2+} affinity in E60Q.

Stability. The calcium form of wild-type calbindin D_{9k} is too stable to denature by heat or chemicals. Therefore, the stability studies were made on the apo forms. The decreased stability toward urea denaturation for (Q22N+P43M) may be explained by the effects on the hydrogen bond network in the β-sheet region observed in the crystal structures and also found in the solution structure both in the presence and in the absence of calcium (*33*). Since this probably could weaken the interaction between the subdomains, it will make the protein more susceptible toward denaturation. The slightly more decreased stability of (Q22E+P43M) could be explained along the same line with the additional effect of an increased negative charge of the protein. This will lead to an increase in repulsion of the subdomains and hence a further decrease in stability. In support of this, N21D has a lower denaturation stability than the wild type. Akke and Forsén (*34*) reported an increase in stability for calbindin D_{9k} mutants when negatively charged, solvent-exposed side chains were changed to uncharged ones.

ACKNOWLEDGMENT

Generous help on stability and stopped-flow experiments by Karin Julenius and Birthe Kragelund is gratefully acknowledged.

REFERENCES

1. Evenäs, J., Malmendal, A., and Forsén, S. (1998) *Curr. Opin. Chem. Biol. 2*, 293−302.
2. Linse, S., and Forsén, S. (1995) *Adv. Second Messenger Phosphoprotein Res. 30*, 89−151.
3. Jalilehvand, F. S. D., Lindqvist-Reis, P., Hermansson, K., Persson, I., and Sandström, M. (2001) *J. Am. Chem. Soc. 123*, 431−441.
4. Ohtaki, H., and Radnai, T. (1993) *Chem. Rev. 93*, 1157−1204.
5. Strynadka, N. C., and James, M. N. (1989) *Annu. Rev. Biochem. 58*, 951−998.
6. Linse, S., Bylsma, N. R., Drakenberg, T., Sellers, P., Forsén, S., Thulin, E., Svensson, L. A., Zajtzeva, I., Zajtsev, V., and Marek, J. (1994) *Biochemistry 33*, 12478−12486.
7. Linse, S., Johansson, C., Brodin, P., Grundström, T., Drakenberg, T., and Forsén, S. (1991) *Biochemistry 30*, 154−162.
8. Henzl, M. T., Hapak, R. C., and Likos, J. J. (1998) *Biochemistry 37*, 9101−9111.
9. Johansson, C., Brodin, P., Grundström, T., Thulin, E., Forsén, S., and Drakenberg, T. (1990) *Eur. J. Biochem. 187*, 455−460.
10. Chazin, W. J., Kördel, J., Drakenberg, T., Thulin, E., Brodin, P., Grundström, T., and Forsén, S. (1989) *Proc. Natl. Acad. Sci. U.S.A. 86*, 2195−2198.
11. Martin, S. R., Andersson Teleman, A., Bayley, P. M., Drakenberg, T., and Forsén, S. (1985) *Eur. J. Biochem. 151*, 543−550.
12. Rance, M., Sørensen, O. W., Bodenhausen, G., Wagner, G., Ernst, R. R., and Wüthrich, K. (1983) *Biochem. Biophys. Res. Commun. 117*, 479−485.
13. Braunschweiler, L., and Ernst, R. R. (1983) *J. Magn. Reson. 53*, 521−528.
14. Shaka, A. L., Lee, C. J., and Pines, A. (1988) *J. Magn. Reson. 77*, 274−293.
15. Kumar, A., Wagner, G., Ernst, R., and Wüthrich, K. (1981) *J. Am. Chem. Soc. 103*, 3654−3658.
16. Gippert, G. P. (1995) Ph.D. Thesis, The Scripps Research Institute, La Jolla, CA.
17. Johansson, C., Ullner, M., and Drakenberg, T. (1993) *Biochemistry 32*, 8429−8438.
18. Merutka, G., Dyson, H. J., and Wright, P. E. (1995) *J. Biomol. NMR 5*, 14−24.
19. Szebenyi, D. M., and Moffat, K. (1986) *J. Biol. Chem. 261*, 8761−8777.
20. Kördel, J., Skelton, N. J., Akke, M., and Chazin, W. J. (1993) *J. Mol. Biol. 231*, 711−734.
21. Kördel, J., Forsén, S., Drakenberg, T., and Chazin, W. J. (1990) *Biochemistry 29*, 4400−4409.
22. Luzzatti, V. (1952) *Acta Crystallogr. 5*, 802−810.
23. Håkansson, M., Svensson, L. A., Fast, J., and Linse, S. (2001) *Protein Sci. 10*, 927−933.
24. Lindhout, M. J., and HC, H. (1978) *Biochim. Biophys. Acta 533*, 318−326.
25. Kesvatera, T., Jönsson, B., Thulin, E., and Linse, S. (1994) *Biochemistry 33*, 14170−14176.
26. Akke, M., Forsén, S., and Chazin, W. J. (1991) *J. Mol. Biol. 220*, 173−189.
27. Carlström, G., and Chazin, W. J. (1993) *J. Mol. Biol. 231*, 415−430.
28. Mäler, L., Blankenship, J., Rance, M., and Chazin, W. J. (2000) *Nat. Struct. Biol. 7*, 245−250.
29. Wesolowski, T. A., Boguta, G., and Bierzynski, A. (1990) *Protein Eng. 4*, 121−124.
30. Biekofsky, R. R., and Feeney, J. (1998) *FEBS Lett. 439*, 101−106.
31. Andersson, M., Malmendal, A., Linse, S., Ivarsson, I., Forsén, S., and Svensson, L. A. (1997) *Protein Sci. 6*, 1139−1147.
32. Martin, S. R., Linse, S., Johansson, C., Bayley, P. M., and Forsén, S. (1990) *Biochemistry 29*, 4188−4193.
33. Skelton, N. J., Forsén, S., and Chazin, W. J. (1990) *Biochemistry 29*, 5752−5761.
34. Akke, M., and Forsén, S. (1990) *Proteins: Struct., Funct., Genet. 8*, 23−29.
35. Linse, S., Thulin, E., and Sellers, P. (1993) *Protein Sci. 2*, 985−1000.
36. Koradi, R., Billeter, M., and Wüthrich, K. (1996) *J. Mol. Graphics 14*, 51−55.

BI010551H